

# Calculation of absolute free energy of binding for theophylline and its analogs to RNA aptamer using nonequilibrium work values

Yoshiaki Tanida,\* Masakatsu Ito, and Hideaki Fujitani

*Fujitsu Laboratories Ltd., 10-1 Morinosato-Wakamiya, Atsugi, Kanagawa, Japan*

(Dated: October 29, 2018)

## Abstract

The massively parallel computation of absolute binding free energy with a well-equilibrated system (MP-CAFEE) has been developed [H. Fujitani, Y. Tanida, M. Ito, G. Jayachandran, C. D. Snow, M. R. Shirts, E. J. Sorin, and V. S. Pande, *J. Chem. Phys.* **123**, 084108 (2005)]. As an application, we perform the binding affinity calculations of six theophylline-related ligands with RNA aptamer. Basically, our method is applicable when using many compute nodes to accelerate simulations, thus a parallel computing system is also developed. To further reduce the computational cost, the adequate non-uniform intervals of coupling constant  $\lambda$ , connecting two equilibrium states, namely bound and unbound, are determined. The absolute binding energies  $\Delta G$  thus obtained have effective linear relation between the computed and experimental values. If the results of two other different methods are compared, thermodynamic integration (TI) and molecular mechanics Poisson-Boltzmann surface area (MM-PBSA) by the paper of Gouda *et al* [H. Gouda, I. D. Kuntz, D. A. Case, and P. A. Kollman, *Biopolymers* **68**, 16 (2003)], the predictive accuracy of the relative values  $\Delta\Delta G$  is almost comparable to that of TI: the correlation coefficients (R) obtained are 0.99 (this work), 0.97 (TI), and 0.78 (MM-PBSA). On absolute binding energies meanwhile, a constant energy shift of  $\sim -7$  kcal/mol against the experimental values is evident. To solve this problem, several presumable reasons are investigated.

---

\*Electronic address: tanida@labs.fujitsu.com

## I. INTRODUCTION

To accurately compute the free energy difference between two thermal equilibrium states ( $\Delta G$ ) is of interest in computational science and of importance in terms of drug discovery [1]. It can help us obtain a quantitative understanding of molecular complexes from atomic-scale, and also provide valuable information for use in structural refinement for drug design. Generally speaking, to discuss chemical reaction, we have to determine the free energy change within so-called chemical accuracy ( $\sim 1$  kcal/mol), which is very challenging. Popularly, several free energy calculations have been carried out within the framework of the thermal equilibrium approach. For instance, free energy perturbation (FEP) [2] and thermodynamic integration (TI) [3] have been widely used to calculate the free energy change associated with the transformation of one ligand into another via thermodynamic cycles [4, 5]. Certainly, the recent improvement in these methods and the increase in computer resources have enabled us to calculate the absolute binding energy concerned with very small organic compounds [6, 7, 8, 9]. However, equilibrium approaches involving most rigorous technique, known as the double decoupling method, require long time simulation to maintain the reversibility about the work associated with the decoupling process. As a more approximate method, the molecular mechanics Poisson-Boltzmann surface area (MM-PBSA) analysis [10] has been a popular method to obtain absolute binding free energies within a reasonable time. In this approach, explicit waters and mobile counter ions are treated by the continuum model after obtaining the molecular dynamics (MD) trajectory. Since the normal mode analysis is time-consuming, the contribution of solute entropy is often approximated based on the average of a few snapshots. On the other hand, in the nonequilibrium statistical approach, Jarzynski recently derived a nonequilibrium work theorem that is valid in far from equilibrium regime [11, 12, 13, 14, 15, 16, 17, 18], although accurate numerical estimates of the exponential average, based on a finite number of sampled works, are relatively difficult [19]. Shirts *et al.* proposed the acceptance ratio (AR) method [20, 21, 22, 23] to estimate the free energy difference and also calculated the binding free energies for eight FKBP12-ligand complexes [24] using the “folding@home” system. Furthermore, our previous work [25] suggested the efficiency of the use of general AMBER force field (GAFF) [26] for ligands to obtain the predictive binding estimates, and simultaneously indicated the importance of starting structures for simulations. In our method the use of many independent compute

nodes or a grid computing system is effective to accelerate simulations, whereupon we also developed a massively parallel computing system, “BioServer”, consisting of 1920 microprocessor elements, to efficiently perform the binding free energy calculations. Hereafter, our method is referred to as the massively parallel computation of absolute binding free energy with a well-equilibrated system (MP-CAFEE).

The principal aim of this study is to explore the practical feasibility of our methodology, based on a nonequilibrium approach. We have performed the calculation of the absolute binding free energy for theophylline and its analogs to the RNA aptamer. On the same system, Gouda *et al.* reported the results of free energy calculations using two different methods, TI and MM-PBSA [27]. Therefore, this system is a good platform to compare the ability between two different methods, namely the equilibrium and nonequilibrium approach. The paper is organized as follows. We initially describe the theoretical background and simulation protocol of binding free energy estimation used through this work, before subsequently explaining the choice of coupling constant  $\lambda$  intervals connecting two equilibrium states in Sec. II. The results for all RNA-ligands are presented and discussed in Sec. III. After pointing out the key features of this system, we conclude in Sec. IV.

## II. COMPUTATIONAL DETAILS

In general, the methods used to calculate the free energy difference in molecular simulations can be classified as either equilibrium or nonequilibrium approaches. Several approaches based on thermal equilibrium, e.g. FEP, TI and the potential of mean force using weighted histogram analysis method with umbrella sampling [28], have been attempted to compute the free energy difference between two equilibrium states. However, the equilibrium approaches encounter the difficulty of removing the nonequilibrium contributions, known as the hysteresis problem [29, 30, 31]. In order to overcome this difficulty, a long time simulation must be performed, to retain the reversibility of quasistatic process associating with the thermal equilibrium. Recently, Jarzynski’s equality exactly relates the free energy difference of two equilibrium states  $i$  and  $j$  to the statistics of works via a nonequilibrium, irreversible process that connects them as  $\exp(-\Delta G/k_B T) = \langle \exp(-W/k_B T) \rangle$ , where  $W$  is the work change of a system from  $i$  to  $j$  under isothermal isobaric (NPT) conditions [32]. A remarkable feature of Jarzynski’s equality is the fact that the switching time between two

states is arbitrary. Subsequently, when the process occurs instantaneously, the work can be defined by the potential energy difference as  $W \equiv U(\lambda_j, \mathbf{x}) - U(\lambda_i, \mathbf{x})$ , where  $U$  and  $\mathbf{x}$  are the potential function and configurational coordinates, respectively. A coupling constant  $\lambda$  is imposed on the path connecting two states. The fluctuation theorem (FT) related with  $P_{i \rightarrow j}(W)$  and  $P_{j \rightarrow i}(W)$  of the work probability distributions along the non-equilibrium forward ( $i \rightarrow j$  direction) and reverse ( $j \rightarrow i$  direction) processes is derived by Crooks [13] as  $P_{i \rightarrow j}(+W)/P_{j \rightarrow i}(-W) = \exp[(W - \Delta G)/k_B T]$ . The ratio between  $P_{i \rightarrow j}(+W)$  and  $P_{j \rightarrow i}(-W)$  depends only the value of the free energy difference  $\Delta G$ . Shirts *et al.* pointed out that the maximum likelihood  $\Delta G$  is given by AR analysis, namely, the control parameter in AR analysis must correspond to the free energy difference [21]. Since two irreversible work distributions in forward and reverse directions cross at  $W = \Delta G$ , both distributions must have a large overlap to obtain the free energy estimate with high accuracy. Subsequently, after applying the multi-staging method, the intermediate stages are inserted onto the path between two states  $i$  and  $j$ , with the total free energy change obtained as the sum of the differences. This type of usage, involving the insertion of many intermediate states on the path connecting two states, seems to be effective. However, since economical issues also play a role because many  $\lambda$  require significant computing resources, we have now addressed the issue concerned with determining the adequate choice of each  $\lambda$  interval. First, potential energy is parameterized by  $\lambda$ , followed by the introduction of the  $\lambda$  dependency to the non-bonded interactions. In order to avoid instability near the end-points of the vanishing atoms through calculation, the non-bonded interaction energy  $U(\lambda^C, \lambda^{LJ})$  between the ligand and others, including the so-called soft-core potentials, is used [33]. We also use two kind of coupling constant  $\lambda$  for representing two different potential energies: the fully bound state ( $\lambda^C = \lambda^{LJ} = 0$ ) and the unbound state ( $\lambda^C = \lambda^{LJ} = 1$ ). Hereafter, the free energy component resulting from turning off the electrostatic potential ( $\lambda^C = 0 \rightarrow 1, \lambda^{LJ} = 0$ ) is referred as the electrostatic contribution. We also denote the free energy component for the process of ( $\lambda^C = 1, \lambda^{LJ} = 0 \rightarrow 1$ ) as the van der Waals contribution. Next, we investigate the convergence properties of the free energy when the number of equal  $\lambda$  spacings ( $\equiv N$ ) increases. A trajectory at each intermediate  $\lambda_i$  is obtained via the standard MD simulation. As already noted, the work associated with the forward path is obtained to compute the potential energy difference as  $W_F(i, i + 1) = U(\lambda_{i+1}, \mathbf{x}_i) - U(\lambda_i, \mathbf{x}_i)$ . Using a trajectory at  $\lambda_{i+1}$ , the work on the reverse path is also obtained as  $W_R(i, i + 1) = U(\lambda_{i+1}, \mathbf{x}_{i+1}) - U(\lambda_i, \mathbf{x}_{i+1})$ , while the free

energy  $\Delta G_{i,i+1}$  can be estimated using both work distributions of  $W_F(i, i+1)$  and  $W_R(i, i+1)$  by the AR algorithm, thus the free energy difference is  $\Delta G = \sum_{i=0}^{N-1} \Delta G_{i,i+1}$ . In general,  $\Delta G$  is being converged as the number of  $N$  increases.  $N_0$  is defined as a large enough number to obtain the well-converged value of  $\Delta G$  ( $\equiv \Delta G_0$ ). We also define  $\Delta G(\lambda_n) = \sum_{i=0}^{n-1} \Delta G_{i,i+1}$ . Finally, to reproduce the feature of  $\Delta G_0(\lambda_n)$ , the adequate mesh points of  $\lambda$  are determined to be satisfied with the following requirements: 1) the small difference between  $\Delta G$  and  $\Delta G_0$ ; 2) the small root mean square (rms) error between  $\Delta G(\lambda_n)$  and  $\Delta G_0(\lambda_n)$ . The rms error used here is defined as  $\left[ (1/N) \sum_{i=0}^{N-1} | \Delta G(\lambda_i) - \Delta G_0(\lambda_i) |^2 \right]^{1/2}$ .

Now, we have applied this manner to an RNA-theophylline system. Using the first 100 ps MD simulation  $N_0$  were determined as 20 for electrostatic contribution and 40 for van der Waals contribution respectively. As can be seen from Table I, we have determined the non-uniform mesh points of  $\lambda$  with  $\Delta G$  difference ( $\equiv \delta G$ )  $\leq 0.05$  kcal/mol and rms error of  $\Delta G(\lambda) \leq 0.1$  kcal/mol, leading to a significant reduction in the number of necessary  $\lambda$  points. The  $\lambda$  points obtained were the following: 12 values of  $\lambda^C$  points (0, 0.1, 0.25, 0.45, 0.55, 0.65, 0.7, 0.75, 0.8, 0.9, 0.95, 1) and 21 values of  $\lambda^{LJ}$  points (0, 0.1, 0.2, 0.275, 0.375, 0.45, 0.55, 0.65, 0.675, 0.725, 0.75, 0.775, 0.8, 0.825, 0.85, 0.875, 0.9, 0.925, 0.95, 0.975, 1). Computed  $\Delta G(\lambda_i)$  as a function of  $\lambda_i$  were also shown in Figs. 1(a) and (b). It is clear that the feature of the well-converged curves is reproduced well by a small number of non-uniform mesh points.

To estimate the free energy difference, the path from the bound state ( $\lambda=0$ ) to the unbound state ( $\lambda=1$ ) is chosen as follows; the ligand electrostatic interactions with the environment are turned off, followed by its van der Waals interactions with the environment, whereupon we obtain the solvation energy of ligand as  $\Delta G_{\text{Solv}} (\equiv \Delta G_{\text{Solv}}^C + \Delta G_{\text{Solv}}^{LJ})$ . The free energy of the annihilation of the ligand from the ligand-receptor complex (complexation free energy) is also calculated as  $\Delta G_{\text{Complex}} (\equiv \Delta G_{\text{Complex}}^C + \Delta G_{\text{Complex}}^{LJ})$ . We schematically note as follows;  $L_{(\text{sol})} \rightarrow L_{(\text{gas})}$  on the calculation of the solvation free energy of the ligand (L) and  $RL_{(\text{sol})} \rightarrow R_{(\text{sol})} + L_{(\text{gas})}$  on the calculation of the complexation free energy of the ligand (L) to the receptor (R). Consequently, we obtain the absolute binding free energy of the receptor-ligand complex as  $\Delta G \equiv \Delta G_{\text{Complex}} - \Delta G_{\text{Solv}} = \Delta G_{\text{Complex}}^C + \Delta G_{\text{Complex}}^{LJ} - \Delta G_{\text{Solv}}^C - \Delta G_{\text{Solv}}^{LJ}$  using the relation of  $RL_{(\text{sol})} \rightarrow R_{(\text{sol})} + L_{(\text{sol})}$ .

In our study the three-dimensional structure of the RNA-theophylline complex proposed by Clore *et al.* [34] (PDB code 1O15) was used as a modeling. We assumed that the bind-

ing sites for six ligands fit into the structural framework of the original RNA-theophylline structure because the structures of other complexes were not experimentally determined. All MD simulations were performed using a modified version of the GROMACS package (v3.1.4) [35] with single precision to speed up the execution. The Amber force field parameters (ff99) were used to describe the RNA aptamer, including 1-4 interactions between hydrogen atoms, while the force field parameters for  $\text{Mg}^{2+}$  ions [36] were also used from the Amber package. The atomic structure of the theophylline molecule was optimized in a vacuum using Gaussian 98 (Gaussian, Inc.) with the HF/6-31G\* single-point energy calculation, while the atomic charges were calculated using the restrained electrostatic potential (RESP) method [37] and the ANTECHAMBER program was used to assign the GAFF for each atom. The chemical structures of the ligands investigated here are shown in Fig. 2, while the electrostatic potential surface of these molecules, computed using the Adaptive Poisson-Boltzmann Solver (APBS) package [38] after using the RESP charge fitting are also shown. It is clear that hypoxanthine has a slightly different charge distribution around the lower left-hand side of the molecule as compared to other molecules. The TIP3P model for water molecules was used to describe the solvent [39].

Through this study we obeyed the following parameters for all MD simulations. Integration of the equation of motion was performed using the leap-frog algorithm and all bonds were constrained by LINCS [40] with order 8. We used the time step of 2.0 fs while the non-bonded pair list of 1 nm was updated every 10 steps. All simulations were carried out at  $T=298$  K using the Nose-Hoover [41, 42] temperature control and at 1 atm using the Berendsen [43] pressure control respectively, with a time constant of 0.5 ps and a compressibility of  $4.5 \times 10^{-5} \text{ bar}^{-1}$ . The particle mesh Ewald (PME) [44] summation was used to evaluate the electrostatic interactions with a grid spacing of approximately 0.12 nm, a cubic spline order of 4 and relative tolerance between long and short range energy of  $10^{-8}$ . The L-J interaction energy was calculated by a switched cutoff between 0.8 nm and 0.9 nm. We also included long range correction to the energy and pressure. We used the truncated octahedron box as a unit cell with periodic boundary conditions, while for the solvated ligand system, we adopted the unit cell size, maintained no closer than 0.85 nm from each face of the box, and introduced about 238 to 282 TIP3P water molecules into the unit cell. RNA-ligand complexes were prepared in which the minimum distance was 0.75 nm between the nearest unit cell wall on either side, while the number of TIP3P water molecules used were either

7192 or 7193. We introduced 3  $\text{Mg}^{2+}$  ions into the complex according to the paper of Gouda *et al* [27, 45, 46] and also added 26  $\text{Na}^+$  counter-ions to the complex to neutralize the system.

One of the difficulties for computing the binding free energy is the preparation of starting structure sampled from the canonical ensemble at the desired temperature  $T$  [25]. The following procedure was used. We performed energy minimization using the conjugate gradient method, followed by the MD simulation of 20 ps relaxation with the solute positions restrained. In order to attain the thermal equilibrium state ( $\lambda^{\text{C}}=\lambda^{\text{LJ}}=0$ ), 10/15 ns MD calculations were typically used for the solvated ligand and the RNA-ligand complexes. Through this process, used to conclude the system to be equilibrated, the total potential energy of the system and the local electrostatic and van der Waals potential energies between RNA and ligand were carefully monitored. Via the multi-stage method we adopted an atomic structure at  $\lambda=0$  after completing the preconditioning MD simulation as a starting structure at each intermediate  $\lambda$  state. To decrease the uncertainty from statistical error, we sampled the MD simulation with 15 and 10 kinds of different initial velocities for the solvated ligand system and RNA-ligand complex, respectively. Nonequilibrium works every 50 steps (0.1 ps) were used to compute the free energies, which were obtained as the arithmetic average of all estimated values. Through this work we simultaneously performed 330 (33 independent non-uniform  $\lambda$  points  $\times$  10 samples) independent MD simulations to generate the energetically possible samples for evaluating the binding free energy on the Fujitsu BioServer system, consisting of 1920 FR-V microprocessors.

### III. RESULTS AND DISCUSSION

It was found that a  $\text{Mg}^{2+}$  ion shielded by water molecules and located at the center of the U-turn formed by C22-U24 [46] remained unchanged during all the preconditioning MD simulations. Conversely however, other  $\text{Mg}^{2+}$  ions immediately left their initial positions, and diffused around an RNA aptamer.

## A. Theophylline

A 15 ns preconditioning MD simulation was used to reach a thermal stable structure in the RNA-theophylline complex. We now consider the energetically favorable structure from the perspective of both electrostatic interaction and that of van der Waals. The obtained structure is consistent as expected, namely, the negative surface region of an RNA strongly interacts with the positive region on a complementary molecule surface. Besides, there is a match of theophylline and residue of A28 on the substrate. This result can be interpreted based on the view that the van der Waals interaction simultaneously stabilizes the theophylline molecule onto the binding pocket. Furthermore, theophylline is bound with an upper as well as lower layer.

Let us now move on to the binding free energy calculation to examine the availability of our method. The open circles in Fig. 3 show the features of the convergence of (a) the solvation free energy of theophylline and of (b) the complexation free energy of theophylline to an RNA as a function of the MD step. Each open circle was obtained by analyzing the generated works during each 100 ps MD trajectory. Rough convergence appears visible after 200 ps and 700 ps for (a) the solvated ligand and (b) the solvated RNA-ligand complex, respectively. Subsequently, we used work values from 200 ps to 1 ns (8000 samples) to estimate the solvation energy  $\Delta G_{\text{Solv}}$  and those from 700 ps to 1 ns (3000 samples) to estimate the complexation energy  $\Delta G_{\text{Complex}}$ , and obtained -14.4 kcal/mol for  $\Delta G_{\text{Solv}}$  and -30.5 kcal/mol for  $\Delta G_{\text{Complex}}$ . Consequently, we also obtained the binding free energy  $\Delta G$  of -16.1 kcal/mol for the RNA-theophylline system. We have summarized the free energy components in Table II and it can be found that the favorable structure of this complex is mainly driven by the van der Waals interaction.

We further comment on the computational cost required to obtain the converged  $\Delta G$ . Since the ratio of the simulation time between the solvation and complexation is relatively small, we only consider the simulation time for obtaining  $\Delta G_{\text{Complex}}$ . In this system, a total of 330 ns MD simulations for obtaining  $\Delta G_{\text{Complex}}$  were used. However, our approach is applicable for the use of many compute nodes to accelerate calculations, meaning the use of a parallel computing system, including a grid environment, is the key to diminishing the computation turnaround time.



## B. Caffeine

Caffeine differs from theophylline by a single methyl group as shown in Fig. 2. Each component, once decomposed from estimated binding energies, was tabulated in Table II. It is evident that the significant difference of 5.1 kcal/mol between the theophylline and caffeine bindings is mainly attributable to the electrostatic contribution (4.6 kcal/mol). We now address and attempt to explore the reason why the affinity between RNA and caffeine is drastically reduced in comparison with that between RNA and theophylline. Due to the typical snapshots, both ligands preferably bind within the pocket of an RNA, as illustrated in Figs. 4(a) and (b). Hereafter, we discuss the results during 1ns MD simulations after reaching thermal equilibrium states for both systems. The obtained averaged distances of TEP(O)-C22(1H4), TEP(hn)-C22(N3), TEP(hn)-C22(O2) and TEP(nc)-U24(H3) are 0.22 nm, 0.19 nm, 0.26 nm and 0.21 nm, respectively, while the averaged distance of CAF(nc)-U24(H3) of 0.21 nm was also obtained for the RNA-caffeine complex. These values indicated the creation of hydrogen bonds as the bond lengths were less than approximately 0.25 nm. This difference in the number of hydrogen bonds between both RNA-caffeine and RNA-theophylline complexes may result in a significant difference in the binding energy, so the number of hydrogen bonds for both systems were enumerated. At this point, we determined the hydrogen bond based on the cutoff angle of the donor-hydrogen-acceptor and the distance of the hydrogen-acceptor; values of  $60^\circ$  for cutoff angle and 0.25 nm for cutoff distance were used. We obtained hydrogen bonds of 4.3 ( $\pm 1.0$ ) for the solvated caffeine and the numerical value in parentheses indicated the standard deviation. On the other hand, the solvated theophylline has 5.4 ( $\pm 1.1$ ) hydrogen bonds. These results indicated a decrease in the hydrogen bond in solvated caffeine as compared to the solvated theophylline. The number of hydrogen bonds for the solvated RNA-caffeine complex were 2.8 ( $\pm 0.8$ ) and 0.9 ( $\pm 0.2$ ) for caffeine-water and RNA-caffeine pairs. We also counted the number of hydrogen bonds for the solvated RNA-theophylline complex: 2.3 ( $\pm 0.7$ ) for theophylline-water and 3.1 ( $\pm 0.6$ ) for RNA-theophylline. This value ( $\sim 3$ ) is easily understood as the hydrogen atom TEP(hn) are shared to be bound by both a nitrogen atom (C22(N3)) and an oxygen atom (C22(O2)) in the solvated RNA-theophylline complex as shown in Fig. 4(a), while these hydrogen bonds vanish in the solvated RNA-caffeine complex in Fig. 4(b). The hydrogen bond contributing to binding energy for the RNA-theophylline system is  $\sim 0$ , while the decrease in the number

of hydrogen bonds for the RNA-caffeine system is  $\sim 0.6$ . The contribution energies to binding free energies are roughly  $\sim 0$  kcal/mol for the RNA-theophylline system and  $\sim 3.6$  kcal/mol for the RNA-caffeine system, based on a presumed hydrogen bond energy of  $\sim 6$  kcal/mol. Therefore, the decrease in the hydrogen bonds represents the main reason for the significant difference in affinity between the RNA-theophylline and RNA-caffeine systems.

### C. Other molecules

To obtain a thermal equilibrium binding structure, we similarly set the initial locations of other molecules in close proximity to the binding site of theophylline for preconditioning MD simulations because the electrostatic potential surface of each molecule is almost the same as theophylline. The obtained stable atomic configurations of other molecules bound with RNA were virtually unchanged. The association of RNA with all six ligands is driven primarily by attractive van der Waals interactions  $\Delta G^{\text{LJ}}$  as tabulated in Table II. The results of the absolute and relative binding free energies we obtained for six ligands are given in Table III, which also tabulates the results of other methods, TI and MM-PBSA [27] and includes three important characteristics: 1) There is an effective linear relation (slope= 1) between the computed absolute binding free energies and experimental ones. We obtained the following relation between the computed relative energies  $\Delta\Delta G_{\text{calc}}$  and experimental ones  $\Delta\Delta G_{\text{expt}}$  for three different methods (the results of TI and MM-PBSA were from Ref. [27]):  $\Delta\Delta G_{\text{calc}} = \Delta\Delta G_{\text{expt}} - 0.1, R = 0.99$  (This work),  $\Delta\Delta G_{\text{calc}} = \Delta\Delta G_{\text{expt}} + 0.19, R = 0.97$  (TI),  $\Delta\Delta G_{\text{calc}} = \Delta\Delta G_{\text{expt}} + 1.68, R = 0.78$  (MM-PBSA), where  $R$  is the correlation coefficient. Consequently, the efficiencies of both our method and the TI method for estimating the relative binding free energies are virtually comparable. Here, we should point out that our method directly estimate the absolute binding energies, whereas the TI method only compute the relative binding energies. We also point out that the absolute binding free energy for the RNA-hypoxanthine system is partly shifted about 1.5 kcal/mol from the linear relation, which means this result might suggest consideration be taken of another binding site for hypoxanthine binding. 2) There is a constant energy shift of  $\sim -7$  kcal/mol from the experimental values  $\Delta G_{\text{expt}}$  as can be seen in Fig. 5. Detailed discussions for the latter are given below.

In general, since water molecules play an important role in free energy calculation, we have

performed calculations of  $\Delta U_{\text{local}}$  as the sum of short-range electrostatic interaction energy and van der Waals interaction energy between RNA and ligand. The sample averaged values during 1 ns MD simulations after reaching the thermal equilibrium state are shown in Fig. 6. In comparison with Fig. 5, our method can reproduce the trend in both 1-methylxanthine and xanthine well, although the large shift ( $\simeq 2$  kcal/mol) from a linear relation between  $\Delta U_{\text{local}}$  and  $\Delta G_{\text{expt}}$  was evident. Consequently, our method evidently takes the effect of water molecules into consideration.

#### D. Constant energy shift

The computed absolute binding free energies were approximately -7 kcal/mol smaller than those obtained by the experiment. How do we solve the puzzle underlying the difference between them? We briefly comment on the presumed reasons to solve this puzzle. First, it is well known that nucleic acid, e.g. RNA or DNA, is generally flexible in solution [47]. There are a number of metastable states in free energy space and long term residence at a single valley, resulting in anomalously slow dynamics. Namely, the ensemble average of several capable atomic structures was observed in the experiment. Thus, in the RNA-theophylline system we examined exploration of another metastable structure using a simulated annealing technique as follows: We first prepared a slightly expanded unit cell that was sufficient to treat the RNA relaxing. Theophylline and RNA aptamer was solvated in a truncated octahedron box with 3  $\text{Mg}^{2+}$  ions, 26  $\text{Na}^+$  counter-ions and 9325 TIP3P water molecules. Next, energy minimization and position restrained MD simulation were carried out in the same manner, as described in II. We also set a simulation temperature of 398 K to disturb the stable complex structure during the simulation time of 100 ps. Consequently, a (meta)stable atomic configuration was obtained by annealing to 298 K. One of the characteristic features was that a  $\text{Mg}^{2+}$  ion leave from the center of the U-turn of C22-U24. Binding free energy of -3.3 kcal/mol was obtained by AR analysis with simulation of up to 1 ns MD, by discarding the first 400 ps runs, which is significantly small compared with the strongly binding structure described in Sec. IIIA. The feature of convergence of the free energy estimation as a function of the MD step for this weakly binding structure was also drawn in Fig. 3. We further divide the binding free energy into electrostatic and van der Waals components. Binding free energy of -0.4 kcal/mol is contributed from the electrostatic part, whereas, -3.0 kcal/mol

is contributed from the van der Waals part. Second, we examined the influence of the atomic charges of the ligand. Here, AM1-BCC charges [48] of the ligand generated from MOPAC2002 were tested.  $\Delta G_{\text{Solv}}$  of -17.7 kcal/mol was obtained, while  $\Delta G_{\text{Complex}}$  of -33.7 kcal/mol was also obtained up to 1 ns MD simulations. Both values increased by  $\sim 3$  kcal/mol as compared to those using RESP charges; hence we obtained binding energy of -15.9 kcal/mol, which is very close to the value of -16.1 kcal/mol using RESP charges. Third, the convergence of binding energy was explored. The solvation energy  $\Delta G_{\text{Solv}}^{\text{LJ}}$  was reduced by approximately 0.5 kcal/mol as the cutoff radius was increased from 0.9 nm to 1 nm. The  $\Delta G_{\text{Complex}}^{\text{LJ}}$  was also reduced by 0.2 kcal/mol as the cutoff radius increased from 0.9 nm to 1 nm, meaning the correction is substantially only 0.3 kcal/mol. Fourth, we previously reported that  $\sim 3$  kcal/mol energy shift from the experimental values is existed in FKBP12-ligand system [25]. Then, several researchers have tried to solve this issue by different approaches [49, 50, 51]. Currently, we believe that this energy shift can be interpreted by the difference of the force field used. The energy shift vanishes when we use the GAFF for representing the potential of the protein to further improve the consistency. Therefore, we examined computing the binding energy using GAFF representing all atoms in the RNA-theophylline system.  $\Delta G_{\text{Solv}}$  of -14.2 kcal/mol was obtained, while  $\Delta G_{\text{Complex}}$  of -27.0 kcal/mol was also obtained, so we obtained a free energy difference  $\Delta G$  of -12.8 kcal/mol. This value still represents an approximate shift from the experimental values by 4.0 kcal/mol. Finally, since an RNA has significant negative charges, we believe the fact that the charge polarizability of an atom is influenced by electrostatic interactions with its surrounding atoms, becomes important [52, 53, 54]. For this reason the polarizable potential model might be considered, however, as the computational cost rises significantly, we have not yet examined this ability. Consequently, this puzzle remains a major challenge in the RNA-ligand system.

#### IV. CONCLUSION

In conclusion, we have introduced the method (MP-CAFEE) as a highly accurate means of obtaining the absolute binding free energy. This method has been applied to investigate the properties of the RNA-ligand system. Since our method is suitable for the use of many compute nodes, we have also developed a massively parallel computing system to

effectively accelerate simulations. To further reduce the computational cost, we determined the adequate non-uniform intervals of two coupling constants and consequently obtained the following details: First, our estimated absolute binding free energies correlate well in terms of a linear fit to the experimental values when all ligands are assumed to be preferable to bind the same binding pocket. By comparing the results of two other methods, TI and MM-PBSA[27], the accuracy of this method is almost comparable to that of TI in terms of relative binding free energy. With this in mind, we believe this method to be a promising tool to quantitatively predict the absolute binding free energy in the drug design domain. Second, we expect a considerable difference in the binding affinity to RNA between theophylline and caffeine to be attributed to the difference in hydrogen bonds of the related environment by analyzing the free energy component. Finally, we find the constant energy of  $\sim -7$  kcal/mol shifted from the experimental values for all ligands on absolute binding free energy. Though considering several presumable solutions to this problem, this area remains incompletely understood.

### Acknowledgments

The authors would like to thank G. Jayachandran, M. R. Shirts, E. J. Sorin, and V. S. Pande for fruitful discussions and also E. Lindahl for help in modifying GROMACS. This work was partly supported by the High-Throughput Biomolecule Analysis System Project of the NEDO (New Energy and Industrial Technology Development Organization, Japan). Three of the authors (H.F., Y.T., and M.I.) would like to thank all the members of the BioServer project in Fujitsu.

- 
- [1] W. L. Jorgensen, *Science* **303**, 1813 (2004).
  - [2] R. W. Zwanzig, *J. Chem. Phys.* **22**, 1420 (1954).
  - [3] J. G. Kirkwood, *J. Chem. Phys.* **3**, 300 (1935).
  - [4] B. L. Tembe and J. A. McCammon, *Comp. Chem.* **8**, 281 (1984).
  - [5] C. F. Wong and J. A. McCammon, *J. Am. Chem. Soc.* **108**, 3830 (1986).
  - [6] M. K. Gilson, J. A. Given, B. L. Bush, and J. A. McCammon, *Biophys. J.* **72**, 1047 (1997).
  - [7] S. Boresch, F. Tettinger, M. Leitgeb, and M. Karplus, *J. Phys. Chem.* **107**, 9535 (2003).

- [8] D. Hamelberg and J. A. McCammon, *J. Am. Chem. Soc.* **120**, 7683 (2004).
- [9] J. Hermans and L. Wang, *J. Am. Chem. Soc.* **119**, 2707 (1997).
- [10] I. Massoval and P. A. Kollman, *J. Am. Chem. Soc.* **121**, 8133 (1999).
- [11] C. Jarzynski, *Phys. Rev. Lett.* **78**, 2690 (1997).
- [12] C. Jarzynski, *Phys. Rev. E* **56**, 5018 (1997).
- [13] G. E. Crooks, *Phys. Rev. E* **61**, 2361 (2000).
- [14] C. Bustamante, J. Liphardt, and F. Ritort, *Physics Today* **58**, 43 (2005).
- [15] G. E. Crooks, *Phys. Rev. E* **60**, 2721 (1999).
- [16] D. Collin, F. Ritort, C. Jarzynski, S. B. Smith, I. Tinoco, and C. Bustamante, *Nature* **437**, 231 (2005).
- [17] J. Liphardt, S. Dumont, S. B. Smith, I. Tinoco, and C. Bustamante, *Science* **296**, 1832 (2002).
- [18] F. Ritort, *Poincare Seminar* **2**, 195 (2003).
- [19] D. A. Hendrix and C. Jarzynski, *J. Chem. Phys.* **114**, 5974 (2001).
- [20] C. H. Bennett, *J. Comput. Phys.* **22**, 245 (1976).
- [21] M. R. Shirts, E. Bair, G. Hooker, and V. S. Pande, *Phys. Rev. Lett.* **91**, 140601 (2003).
- [22] M. R. Shirts and V. S. Pande, *J. Chem. Phys.* **122**, 144107 (2005).
- [23] D. A. Kofke and P. T. Cummings, *Fluid Phase Equilib.* **151**, 41 (1998).
- [24] M. R. Shirts, G. Jayachandran, C. D. Snow, H. Fujitani, E. J. Sorin, and V. S. Pande (unpublished).
- [25] H. Fujitani, Y. Tanida, M. Ito, G. Jayachandran, C. D. Snow, M. R. Shirts, E. J. Sorin, and V. S. Pande, *J. Chem. Phys.* **123**, 084108 (2005).
- [26] J. Wang, R. M. Wolf, J. W. Caldwell, P. A. Kollman, and D. A. Case, *J. Comput. Chem.* **25**, 1157 (2004).
- [27] H. Gouda, I. D. Kuntz, D. A. Case, and P. A. Kollman, *Biopolymers* **68**, 16 (2003).
- [28] S. Kumar, D. Bouzida, R. H. Swendsen, P. A. Kollman, and J. M. Rosenberg, *J. Comp. Chem.* **13**, 1011 (1992).
- [29] T. P. Straatsma, H. J. C. Berendsen, and J. P. M. Postma, *J. Chem. Phys.* **85**, 6720 (1986).
- [30] D. A. Perlman and P. A. Kollman, *J. Chem. Phys.* **90**, 2460 (1989).
- [31] D. A. Perlman and P. A. Kollman, *J. Chem. Phys.* **91**, 7831 (1989).
- [32] S. R. Williams, D. J. Searles, and D. J. Evans, *cond-mat/0611541* (2006).
- [33] M. R. Shirts, Ph. D. dissertation, Stanford University (2005).

- [34] G. M. Clore and J. Kuszewski, *J. Am. Chem. Soc.* **125**, 1518 (2003).
- [35] E. Lindahl, B. Hess, and D. v. d. Spoel, *J. Mol. Model.* **7**, 306 (2001).
- [36] J. Åqvist, *J. Phys. Chem.* **94**, 8021 (1990).
- [37] C. I. Bayly, P. Cieplak, W. D. Cornell, and P. A. Kollman, *J. Phys. Chem.* **97**, 10269 (1993).
- [38] N. Baker, D. Sept, S. Joseph, M. Holst, and J. McCammon, *Proc. Natl. Acad. Sci.* **98**, 10037 (2001).
- [39] W. L. Jorgensen, J. Chandrasekhar, J. D. Madura, R. W. Impey, and M. L. Klein, *J. Chem. Phys.* **79**, 926 (1983).
- [40] B. Hess, H. Bekker, and H. J. C. Berendsen, *J. Comput. Chem.* **18**, 1463 (1997).
- [41] S. Nose, *Mol. Phys.* **52**, 255 (1984).
- [42] W. G. Hoover, *Phys. Rev. A* **31**, 1695 (1985).
- [43] H. J. Berendsen, J. P. Postma, A. DiNola, and J. R. Haak, *J. Chem. Phys.* **81**, 3684 (1984).
- [44] U. Essmann, L. Perera, and M. L. Berkowitz, *J. Chem. Phys.* **103**, 8577 (1995).
- [45] R. D. Jenison, S. C. Gill, A. Pardi, and B. Polisky, *Science* **263**, 1425 (1994).
- [46] G. R. Zimmermann, C. L. Wick, T. P. Shields, R. D. Jenison, and A. Pardi, *RNA* **6**, 659 (2000).
- [47] E. J. Sorin, B. J. Nakatani, Y. M. Rhee, G. Jayachandran, V. Vishal, and V. S. Pande, *J. Mol. Biol.* **337**, 789 (2004).
- [48] A. Jakalian, B. L. Bush, D. B. Jack, and C. I. Bayly, *J. Comput. Chem.* **21**, 132 (2000).
- [49] G. Jayachandran, M. R. Shirts, S. Park, and V. S. Pande, *J. Chem. Phys.* **125**, 084901 (2006).
- [50] D. L. Mobley, J. D. Chodera, and K. A. Dill, *J. Chem. Phys.* **125**, 084902 (2006).
- [51] J. Wang, Y. Deng, and B. Roux, *Biophys. J.* **91**, 2798 (2006).
- [52] L. X. Dang and B. M. Pettitt, *J. Phys. Chem.* **91**, 3349 (1987).
- [53] J. Caldwell, L. X. Dang, and P. A. Kollman, *J. Am. Chem. Soc.* **112**, 9144 (1990).
- [54] M. W. Mahoney and W. L. Jorgensen, *J. Chem. Phys.* **115**, 10758 (2001).

TABLE I: Obtained free energy differences and rms values comparing with well-converged values using condensed equal  $\lambda$  spacings, 20 uniformed points for  $\lambda^C$ , and 40 uniformed points for  $\lambda^{LJ}$  respectively. These values are deduced from the first 100 ps MD trajectory.

	$N$	solvation		complex	
		$\delta G^a$	rms	$\delta G^a$	rms
$\lambda^C$	2	-0.14	0.09	0.08	0.18
	5	0.11	0.09	0.10	0.14
	10	0.03	0.03	0.06	0.07
	11 <sup>b</sup>	0.03	0.03	-0.01	0.03
$\lambda^{LJ}$	2	-6.45	3.73	-10.20	5.89
	5	-2.69	1.16	-2.42	1.19
	10	-0.28	0.13	-1.48	0.60
	20	0.11	0.09	0.27	0.13
	20 <sup>b</sup>	0.05	0.08	-0.05	0.05

<sup>a</sup> $\delta G \equiv \Delta G - \Delta G_0$ , where  $\Delta G_0$  is well-converged value.

<sup>b</sup>These values are obtained using an adaptive  $\lambda$  spacing set (see, in II).

TABLE II: Electrostatic contributions and those of van der Waals, decomposed from obtained binding free energies for each RNA-ligand complex.

Ligand	$\Delta G_{\text{Solv}}$		$\Delta G_{\text{Complex}}$		$\Delta G$	
	$\Delta G_{\text{Solv}}^C$	$\Delta G_{\text{Solv}}^{LJ}$	$\Delta G_{\text{Complex}}^C$	$\Delta G_{\text{Complex}}^{LJ}$	$\Delta G^C$	$\Delta G^{LJ}$
Theophylline	-14.2	-0.2	-19.2	-11.3	-5.0	-11.1
3-Methylxanthine	-16.8	-0.5	-22.1	-9.9	-5.3	-9.4
Xanthine	-19.1	-1.0	-24.8	-10.0	-5.7	-9.0
1-Methylxanthine	-16.7	-0.6	-21.3	-10.2	-4.6	-9.6
Hypoxanthine	-18.2	-0.3	-22.8	-7.2	-4.6	-6.9
Caffeine	-12.7	0.3	-13.1	-10.3	-0.4	-10.6



TABLE III: Absolute binding free energies obtained for RNA aptamer and theophylline and its analogs in kcal/mol.

Ligand	Experiment <sup>a</sup>		TI <sup>b</sup>	MM-PBSA <sup>b</sup>		This work	
	$\Delta G_{\text{exp}}$	$\Delta\Delta G_{\text{exp}}$	$\Delta\Delta G_{\text{bind}}$	$\Delta G_{(\text{MM}+\text{solv})}$	$\Delta\Delta G_{(\text{MM}+\text{solv})}$	$\Delta G_{\text{calc}}$	$\Delta\Delta G_{\text{calc}}$
Theophylline	-8.85	0	0	-18.51	0	-16.1	0
3-Methylxanthine	-7.77	1.08	1.36	-15.27	3.25	-14.7	1.4
Xanthine	-6.91	1.94	1.64	-12.97	5.54	-14.6	1.6
1-Methylxanthine	-6.88	1.97	1.82	-14.24	4.27	-14.2	1.9
Hypoxanthine	-5.87	2.98	—	—	—	-11.6	4.5
Caffeine	-3.35	5.50	6.63	-12.67	5.84	-11.0	5.1

<sup>a</sup>These values are obtained using the formula  $-RT \ln K_d$ , where  $K_d$  is the individual competitor dissociation constant. [45].  $T=298$  K.

<sup>b</sup>These values are from Ref. 27.

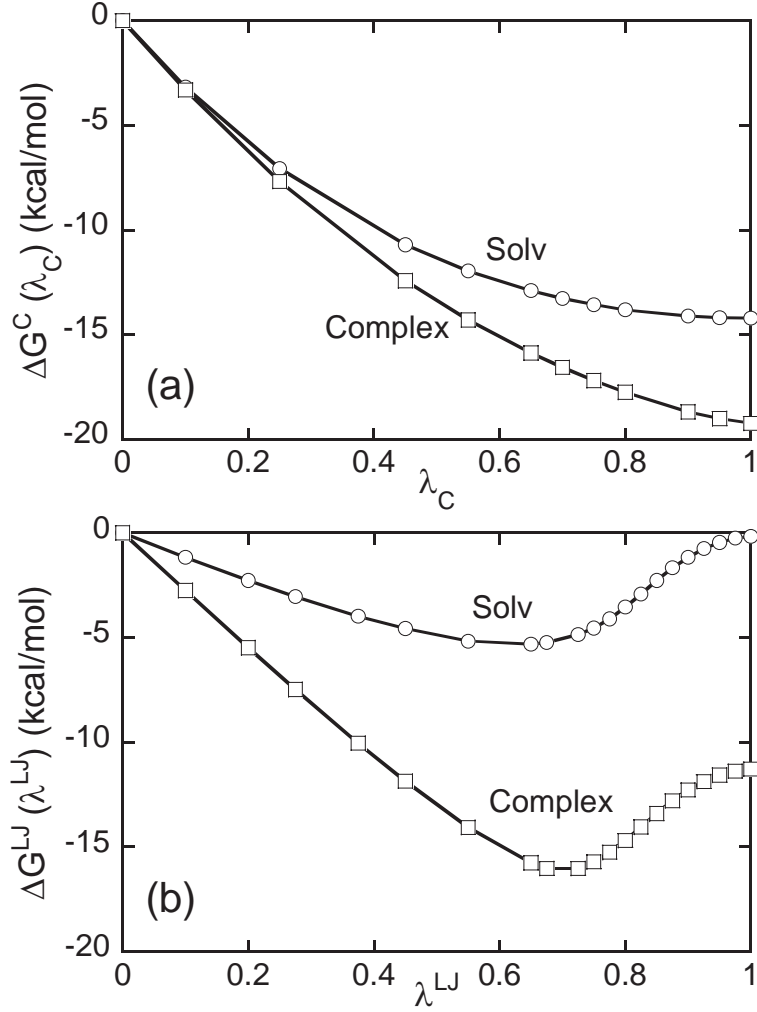


FIG. 1: Free energy convergence as a function of the number of  $\lambda$  spacing for the RNA-Theophylline system; (a)  $\Delta G^C$  vs.  $\lambda^C$ . Open symbols are our reduced 12  $\lambda^C$  points of (0, 0.1, 0.25, 0.45, 0.55, 0.65, 0.7, 0.75, 0.8, 0.9, 0.95, 1). The solid lines are generated from 20 uniform mesh points of  $\lambda^C$ . (b)  $\Delta G^{LJ}$  vs.  $\lambda^{LJ}$ . Open symbols are our reduced 21  $\lambda^{LJ}$  points of (0, 0.1, 0.2, 0.275, 0.375, 0.45, 0.55, 0.65, 0.675, 0.725, 0.75, 0.775, 0.8, 0.825, 0.85, 0.875, 0.9, 0.925, 0.95, 0.975, 1), while the solid lines are generated from 40 uniform mesh points of  $\lambda^{LJ}$ .

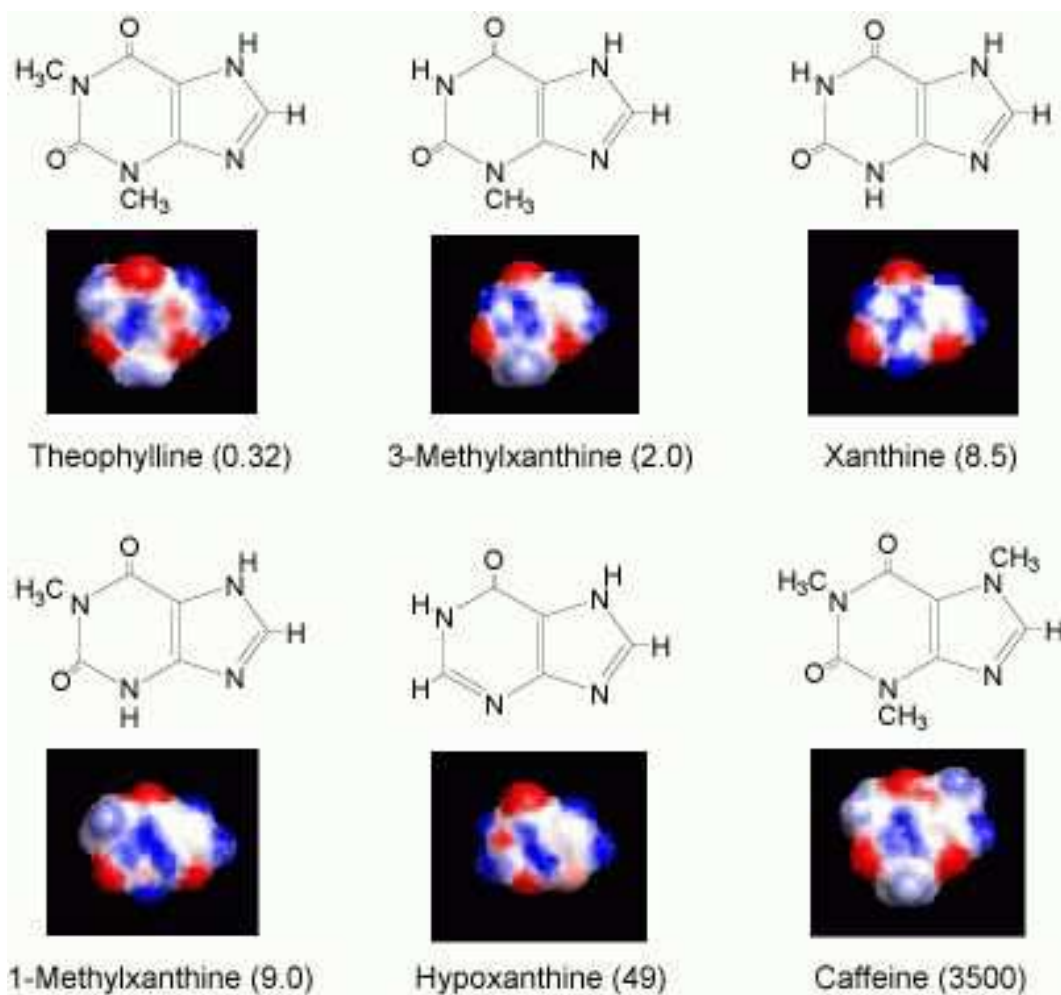


FIG. 2: Chemical structures of ligands investigated. The dissociation constant  $K_d$  (in  $\mu\text{M}$ ) is included in each parenthesis. The electrostatic potential surfaces of molecules are also shown with red representing the negative potential and blue representing the positive potential respectively ( $-4 k_B T/e$  to  $4 k_B T/e$ ).

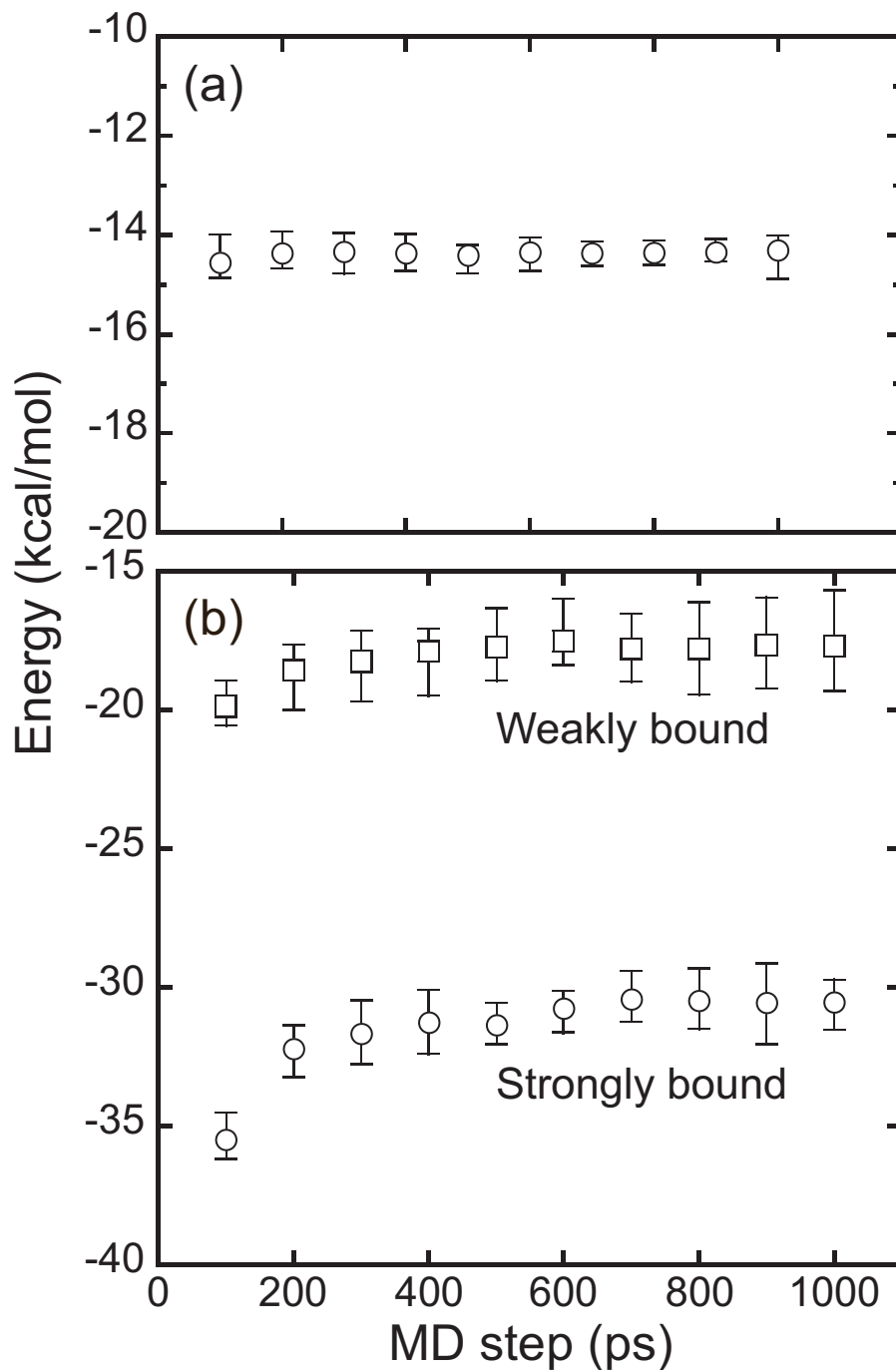


FIG. 3: Free energy of theophylline-RNA aptamer as a function of MD step: (a)  $\Delta G_{\text{Solv}}$  for solvated theophylline, (b)  $\Delta G_{\text{Complex}}$  for the RNA-theophylline complex. Open circle denotes a strongly binding structure, while the open square denotes a weakly binding structure (see, in IIID). Error bars in both graphs are drawn from the maximum value to minimum value.

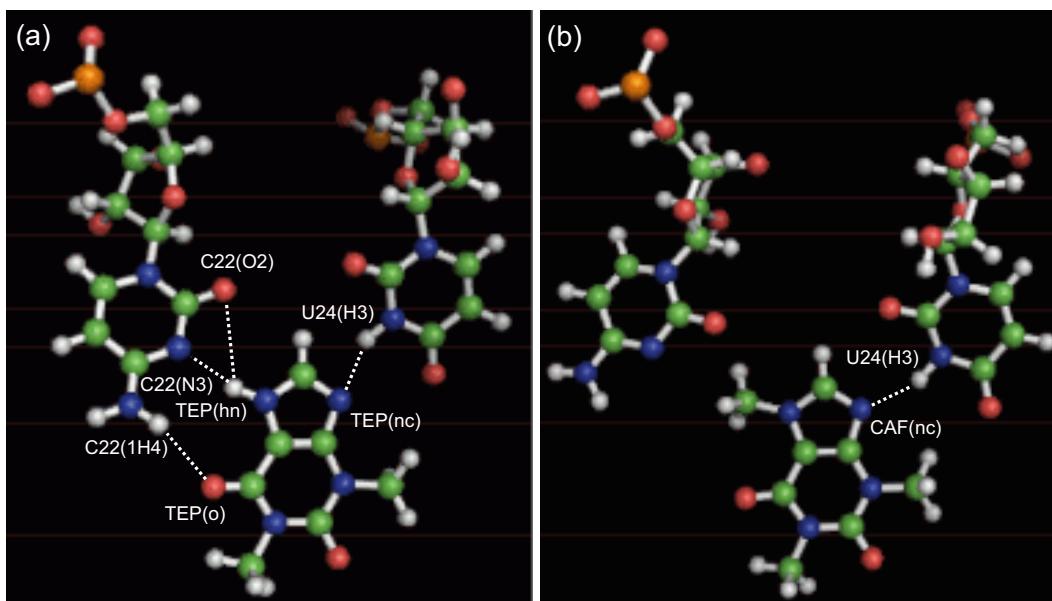


FIG. 4: (a) Theophylline molecule and its surroundings in the RNA-theophylline complex. Only two residues related to hydrogen bonds are drawn and candidates for hydrogen bonds are depicted as dashed lines. (b) Caffeine molecule and its surroundings in the RNA-caffeine complex, while hydrogen bonds with residue in the same plane are also drawn in the form of a dashed line.

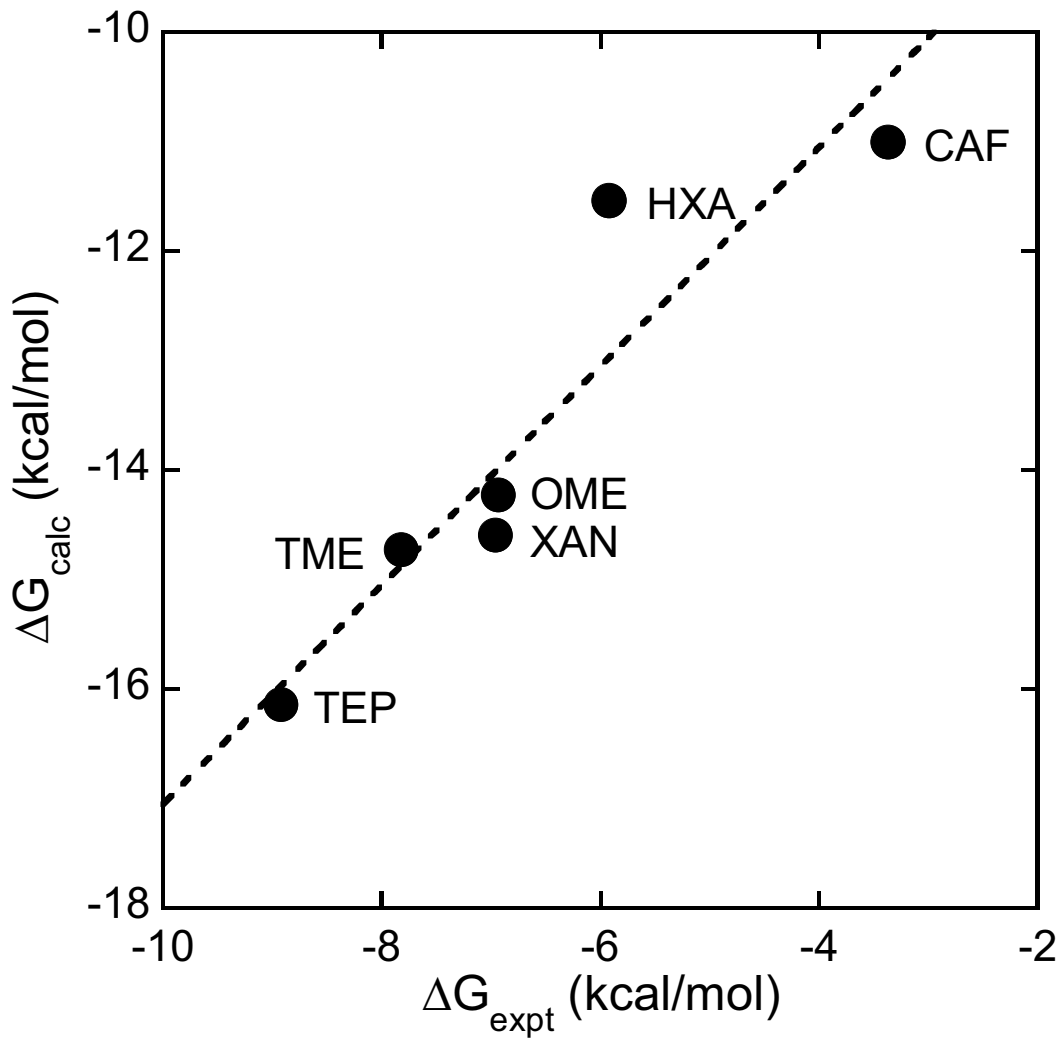


FIG. 5: Computed binding free energies  $\Delta G_{\text{calc}}$  vs. experimentally measured binding free energies  $\Delta G_{\text{expt}}$  for six ligands. The line of slope= 1 is also drawn as a guide. The abbreviations used here are TEP as theophylline, TME as 3-methylxanthine, XAN as xanthine, OME as 1-methylxanthine, HXA as hypoxanthine and CAF as caffeine.

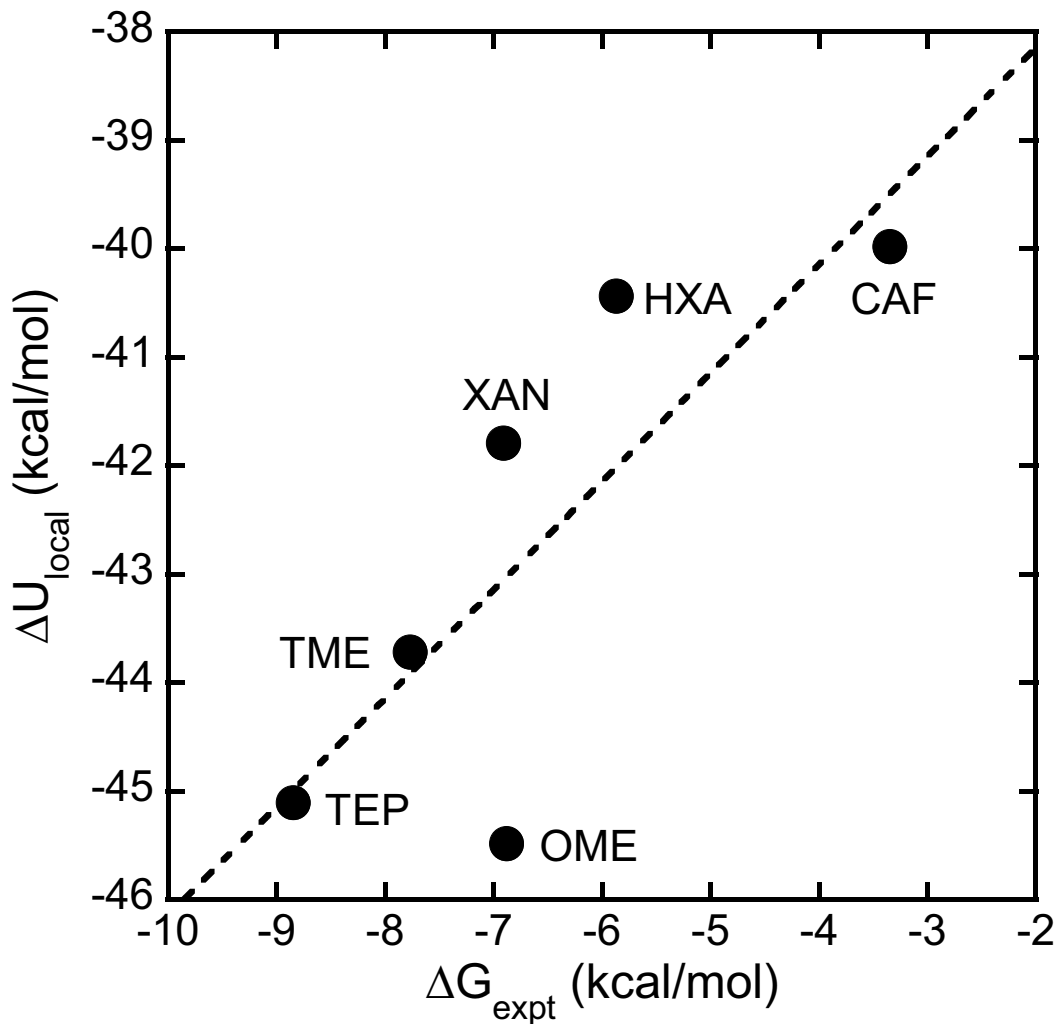


FIG. 6: Local potential energies computed  $\Delta U_{\text{local}}$  vs. experimental binding free energies  $\Delta G_{\text{expt}}$  for six ligands. The line of slope= 1 is also drawn as a guide, while the abbreviations used are the same as those in Fig. 5.